



Get Clarity On Generics

Cost-Effective CT & MRI Contrast Agents

**FRESENIUS
KABI**

[WATCH VIDEO](#)

AJNR

This information is current as
of August 18, 2025.

CT and Multimodal MR Imaging Features of Embryonal Tumors with Multilayered Rosettes in Children

V. Dangouloff-Ros, A. Tauziède-Espariat, C.-J. Roux, R. Levy, D. Grévent, F. Brunelle, A. Gareton, S. Puget, K. Beccaria, T. Blauwblomme, J. Grill, C. Dufour, P. Varlet and N. Boddaert

AJNR Am J Neuroradiol 2019, 40 (4) 732-736

doi: <https://doi.org/10.3174/ajnr.A6001>

<http://www.ajnr.org/content/40/4/732>

CT and Multimodal MR Imaging Features of Embryonal Tumors with Multilayered Rosettes in Children

 V. Dangouloff-Ros,  A. Tauziède-Espariat,  C.-J. Roux,  R. Levy,  D. Grévent,  F. Brunelle,  A. Gareton,  S. Puget,  K. Beccaria,  T. Blauwblomme,  J. Grill,  C. Dufour,  P. Varlet, and  N. Boddart



ABSTRACT

BACKGROUND AND PURPOSE: Embryonal tumors with multilayered rosettes, C19MC-altered, are brain tumors occurring in young children, which were clearly defined in the 2016 World Health Organization classification of central nervous system neoplasms. Our objective was to describe the multimodal imaging characteristics of this new entity.

MATERIALS AND METHODS: We performed a retrospective monocentric review of embryonal brain tumors and looked for embryonal tumors with multilayered rosettes with confirmed C19MC alteration. We gathered morphologic imaging data, as well as DWI and PWI data (using arterial spin-labeling and DSC).

RESULTS: We included 16 patients with a median age of 2 years 8 months. Tumors were both supratentorial (56%, 9/16) and infratentorial (44%, 7/16). Tumors were large (median diameter, 59 mm; interquartile range, 48–71 mm), with absent (75%, 12/16) or minimal (25%, 4/16) peritumoral edema. Enhancement was absent (20%, 3/15) or weak (73%, 11/15), whereas intratumoral macrovessels were frequently seen (94%, 15/16) and calcifications were present in 67% (10/15). Diffusion was always restricted, with a minimal ADC of 520 mm²/s (interquartile range, 495–540 mm²/s). Cerebral blood flow using arterial spin-labeling was low, with a maximal CBF of 43 mL/min/100 g (interquartile range, 33–55 mL/min/100 g 5). When available (3 patients), relative cerebral blood volume using DSC was high (range, 3.5–5.8).

CONCLUSIONS: Embryonal tumors with multilayered rosettes, C19MC-altered, have characteristic imaging features that could help in the diagnosis of this rare tumor in young children.

ABBREVIATIONS: ASL = arterial spin-labeling; ETANTR = embryonal tumors with abundant neuropil and true rosettes; ETMR = embryonal tumors with multilayered rosettes; IQR = interquartile range

The classification of embryonal brain tumors has been redefined in the 2016 World Health Organization classification of central nervous system neoplasms,¹ with the disappearance of the term “primitive neuroectodermal tumors.” Among the newly de-

scribed entities, embryonal tumors with multilayered rosettes, C19MC-altered, were defined by amplification or gain of the C19MC region on chromosome 19 (19q13.42).^{2–4} These tumors include the previously known embryonal tumors with abundant neuropil and true rosettes (ETANTR, also referred to as embryonal tumors with multilayered rosettes [ETMR]), ependymoblastoma, and, in some cases, medulloepithelioma.^{2,4} They can be histopathologically suspected by *LIN28A*-positive immunostaining, but full confirmation warrants molecular confirmation of the C19MC alteration.


Because this type of tumor is rare and was only recently clearly isolated, reports of confirmed C19MC-altered tumors are scarce and most studies did not report detailed imaging data,^{2–14} except for the recent cohort of 7 patients reported by Wang et al.¹⁵ Nowak et al^{16–18} reported imaging data from 22 patients with ependymoblastoma and *LIN28A* immunostaining, but molecular confirmation was absent because these articles were published before the 2016 World Health Organization classification. These reports described ETMRs as large tumors with absent-to-moderate enhancement after contrast media injection and, when DWI


Received October 24, 2018; accepted after revision January 28, 2019.

From the Departments of Pediatric Radiology (V.D.-R., C.-J.R., R.L., D.G., F.B., N.B.) and Pediatric Neurosurgery (S.P., K.B., T.B.), Hôpital Necker Enfants Malades, Paris, France; University René Descartes (V.D.-R., A.T.-E., C.-J.R., R.L., D.G., F.B., S.P., K.B., T.B., P.V., N.B.), Pôle de Recherche et d'Enseignement Supérieur Sorbonne Paris Cité, Paris, France; French National Institute of Health and Medical Research U1000 (V.D.-R., C.-J.R., R.L., D.G., F.B., N.B.), Paris, France; Institut Imagine I163 (V.D.-R., C.-J.R., R.L., D.G., F.B., N.B.), Paris, France; Department of Neuropathology (A.T.-E., A.G., P.V.), Centre Hospitalier Sainte Anne, Paris, France; and Department of Pediatric and Adolescent Oncology (J.G., C.D.), Gustave Roussy Institute, Villejuif, France.

Paper previously presented at: Journées Francophones de Radiologie, October 12–15, 2018, Paris, France.

Please address correspondence to Volodia Dangouloff-Ros, MD, MSc, Assistance-Publique Hôpitaux de Paris, Hôpital Necker-Enfants Malades, Department of Pediatric Radiology, 149 rue de Sèvres, 75015 Paris, France; e-mail: volodia.dangouloff-ros@aphp.fr; @Volodia_DR

 Indicates article with supplemental on-line tables.

 Indicates article with supplemental on-line photos.

<http://dx.doi.org/10.3174/ajnr.A6001>

images were available, a hypersignal on DWI. Nevertheless, because these tumors were rare and gathered during a long time, PWI data and detailed DWI data (such as ADC) were missing.

Our aim was to assess multimodal imaging characteristics of ETMR, C19MC-altered, through a retrospective review of molecularly confirmed cases, including DWI and PWI data.

MATERIALS AND METHODS

Patients

We performed a retrospective review from 2005 to 2018 of the prospective data base of pediatric brain tumors from the Necker Enfants Malades Hospital, Paris, France, as well as a review of the pathology data base. We gathered all tumors previously considered as ependymoblastoma, medulloepithelioma, embryonal tumors with abundant neuropils and true rosettes, and ETMR. They were histopathologically confirmed by an experienced neuropathologist (A.T.-E.) and molecularly confirmed by the presence of a gain or an amplification of C19MC by the CC19MC/TPM4 FISH Probe kit, ref CT-PAC033 (CytoTest; <https://www.cytotest.com/enn/index.asp>). When MR images were available, patients were included in the study.

Ethics committee approval was obtained to study multimodal imaging of children's brain tumors. Agreement of patients was prospectively obtained to perform molecular testing of tumor samples and to use medical images for research purposes.

Imaging

MR imaging was performed at our institution using a Signa HDxt 1.5 T system (GE Healthcare, Milwaukee, Wisconsin) and a 12-channel head-neck-spine coil. Acquired sequences were the following: 3D-T1-weighted, 3D-T2-weighted, FLAIR, DTI, pseudo-continuous 3D-arterial spin-labeling (ASL), DSC if available, and 3D-T1-weighted imaging after contrast media injection. If available, postgadolinium T1-weighted spine imaging was also reviewed. Assessment of calcifications was performed using precontrast CT when available and T2*-weighted sequences (gradient-echo T2 or B₀ of the DWI sequence) otherwise.

Acquisition parameters for the ASL sequence were as follows: TR/TE, 4428/10.5 ms; postlabeling delay, 1025 ms; 80 axial partitions; FOV, 240 × 240 mm; slice thickness, 4 mm; acquisition matrix, 8 spiral arms in each 3D partition with 512 points per arm; flip angle, 155°; acquisition time, 4 minutes 17 seconds. Acquisition parameters for the DTI sequence were the following: 24 directions, b-value = 1000 s/mm², TR = 8000 ms, TE = minimum according to the specific absorption rate, slice thickness = 3 mm, FOV = 240 × 240 mm, matrix size = 512 × 512.

Two senior neuroradiologists (V.D.-R. and R.L.) analyzed MRIs in consensus. Images were qualitatively analyzed using a PACS.

DTI data were analyzed using an Advantage Workstation (Version 4.7; GE Healthcare) to obtain isotropic diffusion maps and average diffusion coefficient maps. ADC, CBF, relative CBF using ASL, and relative CBV using DSC were measured within the whole tumor and within the most diffusion-restricted area or the most perfused area (ROI size, 50 mm²). To obtain relative perfusion values, we used an ROI within the temporal cortex for ASL and a ROI in normal-appearing white matter for DSC.

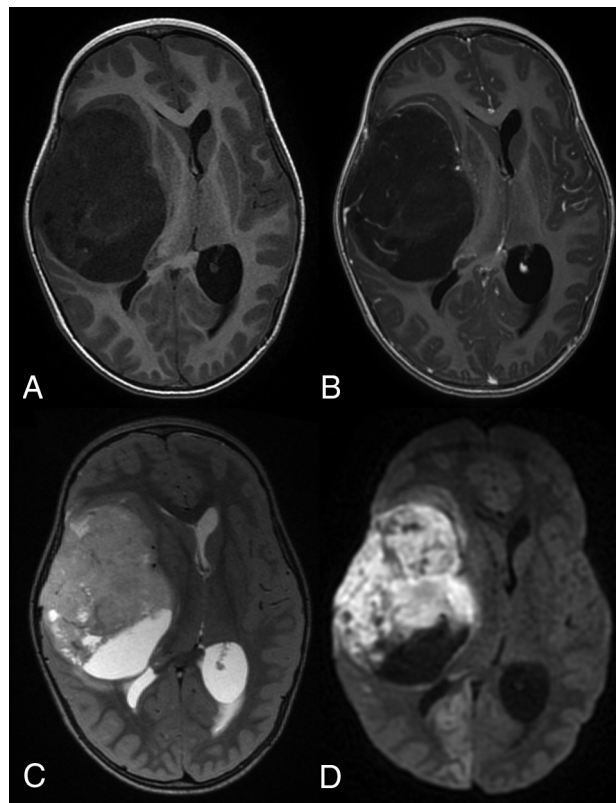


FIG 1. Brain imaging of patient 6. Axial plane MR images show a large heterogeneous right temporal tumor, with mass effect and midline shift. The tumor displays hypointensity on the T1-weighted image (A), hyperintensity on the T2-weighted image (C), and weak enhancement after contrast media injection (B). An intratumoral vessel is seen (B). Diffusion signal is high (D) with low ADC. Diffusion is also restricted in the right occipital lobe (D) because of an ischemic injury caused by compression of the posterior cerebral artery.

Statistical Analysis

Data description was performed using proportions for categorical data and median and interquartile range (IQR) for quantitative data (ADC, CBF, and relative CBF using ASL, relative CBV and relative CBF using DSC).

RESULTS

Patients

Among 2568 patients in the data base, 22 patients with suspected ETMR were histopathologically reviewed. Sixteen patients (12 girls, 4 boys) with ETMR, C19MC-altered, were included, with a median age of 2 years 8 months (range, 1 year 2 months to 11 years 10 months).

Imaging

Findings are reported in On-line Table 1 and On-line Table 2.

Both MR imaging and CT scans were available for 9/16 patients; 6/16 had only MR images, whereas 1/16 had only CT images (patient 14, who died within 1 day of her admission in the hospital). DWI with ADC was available for 13/16 patients; ASL, for 8/16 patients; and DSC, for 3/16 patients. Spinal imaging was available for 7/16 patients.

Tumors were always intra-axial, supratentorial in 9 cases (within hemispheres with variable involvement of the basal gan-

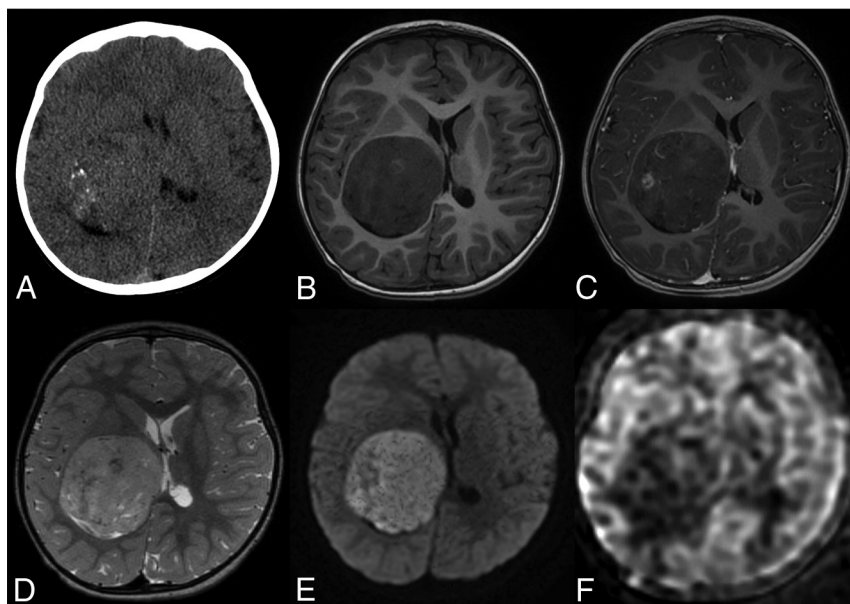


FIG 2. Brain imaging of patient 11. Axial plane image on CT (A) shows a right thalamic mass with microcalcifications. The tumor displays hypointensity on the T1-weighted image (B), hyperintensity on the T2-weighted image (D), and weak nodular enhancement after contrast media injection (C). An intratumoral vessel is seen (C). Diffusion signal is high (E) with low ADC. Cerebral blood flow (F) is low (maximum, 46 mL/min/100 g) within the tumor.

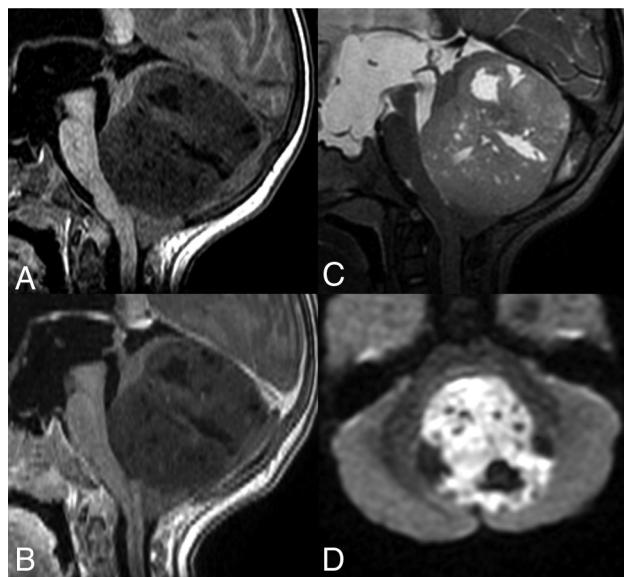


FIG 3. Brain imaging of patient 3. Sagittal plane (A–C) MR images show a large midline vermian tumor, with mass effect on the fourth ventricle causing hydrocephalus. The tumor displays hypointensity on the T1-weighted image (A), hyperintensity on the T2-weighted image (C), and no enhancement after contrast media injection (B). Diffusion signal is high (D) with low ADC.

glia) (Figs 1 and 2) and infratentorial in 7 cases (2 lateralized within the tentorial incisura, equally supra- and infratentorial, posterior and lateral to the cerebral peduncle, with mass effect on the cerebral peduncle [On-line Fig 1]; 2 in the cerebellar vermis [Fig 3]; 1 in the fourth ventricle; and 2 within the brain stem [Fig 4 and On-line Fig 2]). Their median largest diameter was 59 mm (IQ, 48–71 mm), causing mass effect and frequent brain herniation. Peritumoral edema was rare (4/16) and not very extended when present.

No intracranial dissemination was seen at diagnosis, nor spinal metastasis when spine MR imaging was available.

Calcifications were present in 67% (10/15, Fig 2), and tumor density on CT was variable, though more frequently hyperdense (5/10). Tumors were always hypointense on T1-weighted images and hyperintense on T2-weighted and FLAIR images. Enhancement was weak and heterogeneous, sometimes nodular, except for the older patient (patient 16, 11 years of age) in whom the tumor had high and homogeneous enhancement. All patients except 1 (patient 15, On-line Fig 2) had curvilinear homogeneous enhancement connected to cortical veins, consistent with large intratumoral macroscopic veins (diameter, 1–2.5 mm).

Diffusion was always restricted, with a median minimal ADC measured at 520 mm^2/s (IQR 495–540 mm^2/s) and a median ADC within the whole tumor of 728 mm^2/s (IQR, 611–802 mm^2/s).

CBF using ASL was low, with a median value within the most perfused area of 43 mL/min/100 g (IQR, 33–55 mL/min/100 g) and a median value within the whole tumor of 30 mL/min/100 g (IQR, 24–40 mL/min/100 g). DSC-PWI was performed for only 3 patients (between 2 and 3 years of age) and showed high maximal and mean relative CBV (range, 3.5–5.8, and 1.7–2.7, respectively; On-line Table 2). DSC-derived relative CBF was also high (maximal range and mean range, 2.6–4.4 and 1.1–1.9, respectively).

DISCUSSION

In this cohort, we report the characteristic imaging features of confirmed ETMR, C19MC-altered: large tumors with frequent calcifications, little-to-no edema, absent or weak contrast enhancement, intratumoral veins, restricted diffusion, and low CBF values using ASL.

Fifty-six percent of the tumors were hemispheric with variable basal ganglia involvement. This is slightly lower than previous larger clinical or pathologic cohorts, which reported 70%–76% supratentorial tumors.^{2–4,13,16} The distribution of posterior fossa tumors between the fourth ventricle/cerebellum and brain stem was also reported.^{3,15,16} Most interesting, we found 2 tumors lateralized within the tentorial incisura, equally supra- and infratentorial, posterior and lateral to the cerebral peduncle, with mass effect on the cerebral peduncle, which has rarely been reported.^{19–21} Nevertheless, because previous articles reported few imaging details, these tumors may have been classified as posterior fossa tumors or superior cerebellum vermis tumors. Their anatomic localization was difficult to define because of their large size.

Weak contrast enhancement is quite an original feature for this high-grade neoplasm and supports contrast enhancement not being a criterion for high-grade tumors in children.²² This absent or min-

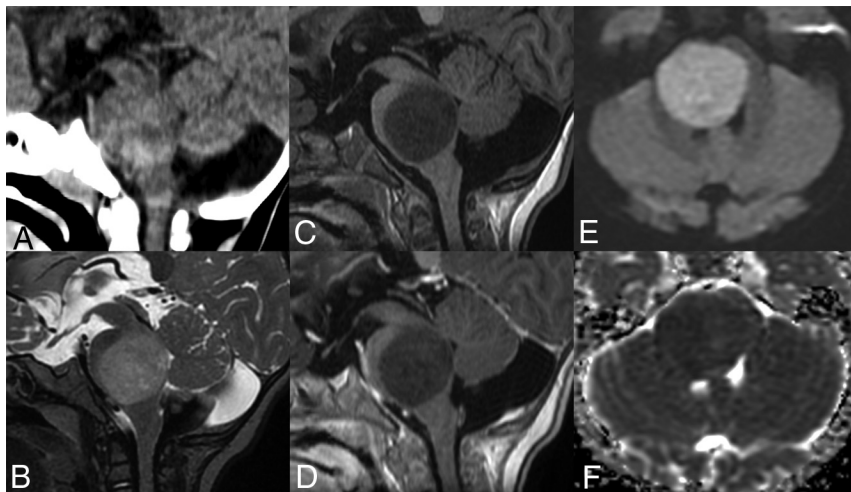


FIG 4. Brain imaging of patient 4. Sagittal plane image on CT (A) shows a pontine isodense mass. The tumor displays hypointensity on the T1-weighted image (C), hyperintensity on the T2-weighted image (B), and no enhancement after contrast media injection (D). Diffusion signal is high (E) with low ADC (F).

imal enhancement was also reported in several cases of confirmed ETMR^{6,9,12,14,15} and in the *LIN28A*-stained ependymoblastoma cohort published by Nowak et al.¹⁶ The only outlier (patient 16) who had high contrast enhancement was clearly atypical because this patient was by far the oldest (11 years of age) and had high CBF. On the other hand, intratumoral large vessels were seen in all patients except 1 (patient 15, who had a mostly cystic tumor with peripheral tissular content). This feature was not detailed in previous reports, except in a few cases reports of histopathologically diagnosed ETANTR.^{23–26}

Diffusion was restricted in all tumors, with a median ADC of 728 mm²/s for the whole tumor and 520 mm²/s for the area of maximum diffusion restriction. Hypersignal on DWI in confirmed ETMR was also previously reported,^{12,15} as well as in the ependymoblastoma cohort of Nowak et al,¹⁶ but no ADC values have been reported yet. This result is in line with the classic diffusion restriction in embryonal tumors in children, formerly known as primitive neuroectodermal tumors.²⁷

CBF using ASL was low (ie, <50 mL/min/100 g) for most patients, with a median maximal CBF of 43 mL/min/100 g. To our knowledge, no previous PWI data were reported. This feature may be surprising for these high-grade neoplasms because high-grade pediatric tumors usually have high CBF using ASL.^{22,28–31} However, this is consistent with the study of Danguloff-Ros et al²² on the posterior fossa, which reported that tumors with a moderate CBF (25–50 mL/min/100 g) but a weak contrast enhancement were high-grade neoplasms, including embryonal tumors. This CBF/enhancement ratio was not reported in hemispheric tumors, but supratentorial embryonal tumors (former primitive neuroectodermal tumors) were absent in this cohort.

Relative CBV using DSC was available for only 3 patients; it has become less frequently used in our institution after the introduction of the ASL sequence because it requires contrast media injection with high flow, which is difficult to obtain in young children. Relative CBV was high in all 3 cases (range, 3.5–5.8), even if CBF using ASL was as low as in other patients. This finding underlines the different pathophysiologic mechanisms involved in ASL and DSC PWI.³² The presence of calcifications in 2 of these

patients (CT not available for the third patient) may have caused artifacts while using DSC and consequently less consistent results.

These homogeneous imaging characteristics may help to distinguish ETMR from other brain tumors in children between 1 and 4 years of age. Pilocytic astrocytoma is quite easily differentiated because it has no diffusion restriction and strong contrast enhancement.³³ Ependymoma differs by its morphology, T2-weighted high signal, and variable DWI pattern.^{18,33} Most of all, some characteristics may be useful to distinguish ETMR from other embryonal brain tumors (ie, medulloblastoma and atypical teratoid/rhabdoid tumor, which may look like ETMR because they are aggressive tumors with high cellularity

causing diffusion restriction).^{33,34} ETMR localization was different from that of classic medulloblastomas because it was not localized in the fourth ventricle (except in the one 11-year-old outlier patient). When localized in the cerebellar hemispheres (Sonic Hedgehog subgroup), medulloblastomas are different again because this subgroup has high contrast enhancement.³⁴ Contrast uptake of ETMR was low, contrary to reported data concerning atypical teratoid/rhabdoid tumors.³⁵ Furthermore, atypical teratoid/rhabdoid tumors usually have a much more necrotic pattern, with central cysts,³⁵ than that in our ETMR cohort. Finally, medulloblastomas and atypical teratoid/rhabdoid tumors usually have high cerebral blood flow using ASL.²²

Our study has several limitations. DSC was performed in only 3/16 patients, and one should use caution generalizing our relative CBV values. Also, we did not have spectroscopy data within the tumor because spectroscopy was not routinely performed in our institution.

CONCLUSIONS

We report the imaging data of 16 patients with confirmed ETMR, C19MC-altered. Imaging features were characteristic and should help to diagnose these rare tumors in young children between 1 and 4 years of age.

Disclosures: Jacques Grill—UNRELATED: Expert Testimony: Hoffmann-La Roche*; Grants/Grants Pending: Bristol-Myers Squibb, Novartis, Roche.* Pascale Varlet—UNRELATED: Consultancy: Hoffmann-La Roche Novartis*; Grants/ Grants Pending: Boehringer Ingelheim. *Money paid to the institution.

REFERENCES

- Louis DN, Perry A, Reifenberger G, et al. **The 2016 World Health Organization Classification of Tumors of the Central Nervous System: a summary.** *Acta Neuropathol (Berl)* 2016;131:803–20 [CrossRef Medline](#)
- Korshunov A, Sturm D, Ryzhova M, et al. **Embryonal tumor with abundant neuropil and true rosettes (ETANTR), ependymoblastoma, and medulloepithelioma share molecular similarity and comprise a single clinicopathological entity.** *Acta Neuropathol (Berl)* 2014;128:279–89 [CrossRef Medline](#)
- Korshunov A, Remke M, Gessi M, et al. **Focal genomic amplification at 19q13.42 comprises a powerful diagnostic marker for embryonal**

- tumors with ependymoblastic rosettes. *Acta Neuropathol (Berl)* 2010;120:253–60 [CrossRef Medline](#)
4. Spence T, Sin-Chan P, Picard D, et al. CNS-PNETs with C19MC amplification and/or LIN28 expression comprise a distinct histogenetic diagnostic and therapeutic entity. *Acta Neuropathol (Berl)* 2014;128:291–303 [CrossRef Medline](#)
 5. Ryzhova MV, Zheludkova OG, Ozerov SS, et al. A new entity in WHO classification of tumors of the central nervous system—embryonic tumor with abundant neuropil and true rosettes: case report and review of literature. *Zh Vopr Neirokhir Im N N Burdenko* 2011;75:25–33
 6. Woehrer A, Slavic I, Peyrl A, et al. Embryonal tumor with abundant neuropil and true rosettes (ETANTR) with loss of morphological but retained genetic key features during progression. *Acta Neuropathol (Berl)* 2011;122:787–90 [CrossRef Medline](#)
 7. Kleinschmidt-DeMasters BK, Boylan A, Capocelli K, et al. Multinodular leptomeningeal metastases from ETANTR contain both small blue cell and maturing neuropil elements. *Acta Neuropathol (Berl)* 2011;122:783–85 [CrossRef Medline](#)
 8. Nobusawa S, Orimo K, Horiguchi K, et al. Embryonal tumor with abundant neuropil and true rosettes with only one structure suggestive of an ependymoblastic rosette. *Pathol Int* 2014;64:472–77 [CrossRef Medline](#)
 9. Hervey-Jumper SL, Altshuler DB, Wang AC, et al. The role of CD133+ cells in a recurrent embryonal tumor with abundant neuropil and true rosettes (ETANTR). *Brain Pathol* 2014;24:45–51 [CrossRef Medline](#)
 10. Gessi M, Demir H, Goschzik T, et al. MET T992I mutation in a case of ependymoblastoma/embryonal tumour with multilayered rosettes. *J Clin Pathol* 2014;67:1017–18 [CrossRef Medline](#)
 11. Antonelli M, Korshunov A, Mastronuzzi A, et al. Long-term survival in a case of ETANTR with histological features of neuronal maturation after therapy. *Virchows Arch* 2015;466:603–07 [CrossRef Medline](#)
 12. Sato H, Terakawa Y, Tsuyuguchi N, et al. Embryonal tumor with abundant neuropil and true rosettes in the brainstem: case report. *J Neurosurg Pediatr* 2015;16:291–95 [CrossRef Medline](#)
 13. Horwitz M, Dufour C, Leblond P, et al. Embryonal tumors with multilayered rosettes in children: the SFCE experience. *Childs Nerv Syst* 2016;32:299–305 [CrossRef Medline](#)
 14. Tariq MU, Ahmad Z, Minhas MK, et al. Embryonal tumor with multilayered rosettes, C19MC-altered: report of an extremely rare malignant pediatric central nervous system neoplasm. *SAGE Open Med Case Rep* 2017;5:2050313X17745208 [CrossRef Medline](#)
 15. Wang B, Gogia B, Fuller GN, et al. Embryonal tumor with multilayered rosettes, C19MC-altered: clinical, pathological, and neuroimaging findings. *J Neuroimaging* 2018;28:483–89 [CrossRef Medline](#)
 16. Nowak J, Seidel C, Berg F, et al. MRI characteristics of ependymoblastoma: results from 22 centrally reviewed cases. *AJNR Am J Neuroradiol* 2014;35:1996–2001 [CrossRef Medline](#)
 17. Nowak J, Seidel C, Pietsch T, et al. Ependymoblastoma of the brainstem: MRI findings and differential diagnosis. *Pediatr Blood Cancer* 2014;61:1132–34 [CrossRef Medline](#)
 18. Nowak J, Seidel C, Pietsch T, et al. Systematic comparison of MRI findings in pediatric ependymoblastoma with ependymoma and CNS primitive neuroectodermal tumor not otherwise specified. *Neuro Oncol* 2015;17:1157–65 [CrossRef Medline](#)
 19. Maiti TK, Arimappamagan A, Mahadevan A, et al. Rare pathologies in the posterior third ventricular region in children: case series and review. *Pediatr Neurosurg* 2015;50:42–47 [CrossRef Medline](#)
 20. Al-Hussaini M, Abuirmelch N, Swaidan M, et al. Embryonal tumor with abundant neuropil and true rosettes: a report of three cases of a rare tumor, with an unusual case showing rhabdomyoblastic and melanocytic differentiation. *Neuropathology* 2011;31:620–25 [CrossRef Medline](#)
 21. Ferri Niguez B, Martínez-Lage JF, Almagro M-J, et al. Embryonal tumor with abundant neuropil and true rosettes (ETANTR): a new distinctive variety of pediatric PNET—a case-based update. *Childs Nerv Syst* 2010;26:1003–08 [CrossRef Medline](#)
 22. Dangouloff-Ros V, Deroulers C, Foissac F, et al. Arterial spin labeling to predict brain tumor grading in children: correlations between histopathologic vascular density and perfusion MR imaging. *Radiology* 2016;281:553–66 [CrossRef Medline](#)
 23. Dunham C, Sugo E, Tobias V, et al. Embryonal tumor with abundant neuropil and true rosettes (ETANTR): report of a case with prominent neurocytic differentiation. *J Neurooncol* 2007;84:91–98 [CrossRef Medline](#)
 24. Manjila S, Ray A, Hu Y, et al. Embryonal tumors with abundant neuropil and true rosettes: 2 illustrative cases and a review of the literature. *Neurosurg Focus* 2011;30:E2 [CrossRef Medline](#)
 25. Adamek D, Sofowora KD, Cwiklinska M, et al. Embryonal tumor with abundant neuropil and true rosettes: an autopsy case-based update and review of the literature. *Childs Nerv Syst* 2013;29:849–54 [CrossRef Medline](#)
 26. Govindan A, Vp M, Alapatt JP. Embryonal tumor with multilayered rosettes in a 3-year-old girl: case report. *Turk Neurosurg* 2017 Jan 8. [Epub ahead of print] [CrossRef Medline](#)
 27. Shih RY, Koeller KK. Embryonal tumors of the central nervous system: from the radiologic pathology archives. *Radiographics* 2018;38:525–41 [CrossRef Medline](#)
 28. Yeom KW, Mitchell LA, Lober RM, et al. Arterial spin-labeled perfusion of pediatric brain tumors. *AJNR Am J Neuroradiol* 2014;35:395–401 [CrossRef Medline](#)
 29. Kikuchi K, Hiwatashi A, Togao O, et al. Correlation between arterial spin-labeling perfusion and histopathological vascular density of pediatric intracranial tumors. *J Neurooncol* 2017;135:561–69 [CrossRef Medline](#)
 30. Morana G, Piccardo A, Tortora D, et al. Grading and outcome prediction of pediatric diffuse astrocytic tumors with diffusion and arterial spin labeling perfusion MRI in comparison with 18F-DOPA PET. *Eur J Nucl Med Mol Imaging* 2017;44:2084–93 [CrossRef Medline](#)
 31. Morana G, Tortora D, Staglianò S, et al. Pediatric astrocytic tumor grading: comparison between arterial spin labeling and dynamic susceptibility contrast MRI perfusion. *Neuroradiology* 2018;60:437–46 [CrossRef Medline](#)
 32. Vidyasagar R, Abernethy L, Pizer B, et al. Quantitative measurement of blood flow in paediatric brain tumours: a comparative study of dynamic susceptibility contrast and multi time-point arterial spin labelled MRI. *Br J Radiol* 2016;89:20150624 [CrossRef Medline](#)
 33. Plaza MJ, Borja MJ, Altman N, et al. Conventional and advanced MRI features of pediatric intracranial tumors: posterior fossa and suprasellar tumors. *Am J Roentgenol* 2013;200:1115–24 [CrossRef Medline](#)
 34. Dangouloff-Ros V, Varlet P, Levy R, et al. Imaging features of medulloblastoma: conventional imaging, diffusion-weighted imaging, perfusion-weighted imaging, and spectroscopy—from general features to subtypes and characteristics. *Neurochirurgie* 2018 Aug 28. [Epub ahead of print] [CrossRef Medline](#)
 35. Au Yong KJ, Jaremko JL, Jans L, et al. How specific is the MRI appearance of supratentorial atypical teratoid rhabdoid tumors? *Pediatr Radiol* 2013;43:347–54 [CrossRef Medline](#)